Marine Hydrokinetic Turbine Blade Fault Signature Analysis using Continuous Wavelet Transform

Brittny Freeman*, Yufei Tang*, and James VanZwieten†
* Department of Computer & Electrical Engineering and Computer Science
† Southeast National Marine Renewable Energy Center
Florida Atlantic University, Boca Raton, FL 33431, USA
Email: {bfreem10, tangy, jvanzwi}@fau.edu

***Abstract*—This paper analyzes the impacts that hydrodynamic asymmetry faults have on marine hydrokinetic (MHK) turbines and the challenges encountered when seeking to identify these faults using non-intrusive fault detection and condition monitoring methods. When hydrodynamic asymmetry faults occur, they induce vibrational kinetic energy upon the turbine's rotor shaft at a frequency equal to the rotational frequency of the low speed shaft (1P frequency). This vibrational energy is difficult to visualize when observing the frequency spectrum of generator's electrical power when only using FFT and windowed FFT signal processing methods. Such difficulties are a consequence of the low signal to noise ratio (SNR) and non-stationary nature of the generator's electrical power signals. This paper utilizes a continuous wavelet transform (CWT) with a complex Morlet wavelet basis function to identify and quantify vibrational frequency excitations contained within the generator's output power, with an aim towards performing machine condition monitoring and fault detection on MHK turbines.**

I. Introduction

According to the National Renewable Energy Laboratory's (NREL) Renewable Electricity Futures Study, it will be technically feasible for 80% of all U.S. electricity production to be generated from renewable energy sources by 2050 [1], [2]. As efforts ramp up to meet this goal, the demand for clean and renewable electricity generation from sources outside of conventional wind and solar will likely increase dramatically. Tidal, river, and ocean currents represent highly concentrated renewable sources of energy that are both reliable and sustainable. It has been estimated that energy extraction in US waters from just the Gulf Stream current alone has the potential to generate up to 18.6 GW (163 TWh/yr) of electrical power [3]. Unfortunately, due in part to economic concerns relating to the currently high levelized cost of energy (LCOE) associated with this form of renewable energy generation, mainstream efforts to widely implement the technologies needed to harness these energy sources remain in their infancy.

This research proposes a promising means of lowering the LCOE associated with marine hydrokinetic (MHK) turbine usage through O&M cost reduction. This approach analyzes the frequency spectrum of the turbine's generator electrical power to determine if excitations at the 1P shaft rotating frequency can be statistically quantified to reveal any relevant fault detection information. The 1P frequency is the frequency of rotation of the turbine's low speed shaft, for which a continuous wavelet transform (CWT) that incorporates a complex Morlet wavelet basis function, is used to quantify the vibrational excitation energy induced upon the low speed shaft.

The 1P shaft rotating frequency has been successfully used in [4] to visually locate wind turbine imbalance faults within plots of the power spectral density (PSD) of the rotor shaft's frequency spectrum. In [5], Gong *et al*. proposed an interpolation/up-sampling then down-sampling algorithm to convert the non-stationary fundamental frequency of the stator current into a more stationary version of itself. This allowed for the characteristic frequencies of inner and outer-race bearing faults to be more readily identified in the PSD of the stator current.

In addition to these works, more generalized surveys have been performed, specifically aimed at rotating machine fault detection (RMFD) and condition monitoring techniques. In particular, a survey focused on fault diagnostic techniques targeted at induction machines subjected to non-stationary loads and speeds was published by Guasp *et al* [6]. In Guasp's work, different diagnosis methods are summarized and categorized by domain so that conceptual and practical understandings of their implementations can be achieved. With respect to wavelet transforms, a survey reviewing recent publications that utilized wavelets for rotary machine fault diagnosis was presented by Yan *et al*. [7]. Yan summarized works dealing with fault diagnostic applications according to specific categories of the wavelet transform, including but not limited to the CWT, discrete wavelet transforms (DWT), wavelet packet transforms (WPT), second generation wavelet transforms, and dual-tree complex wavelet transforms. An in-depth and comprehensive review on the importance of the inner product operation contained within the wavelet transforms in reference to fault feature detection for rotating machinery is presented by Chen et al. [8]. Chen's work investigates the influences that the use of the inner product principle has had on major developments in wavelet RMFD. Lastly, Cohen formulated improved ways of parameterizing Morlet Wavelets so that accurate analyses, reporting, and interpretation of their results can be achieved [9].

The remainder of the paper is structured as follows. Section II briefly describes the simulation platform and presents background information on the nature of hydrodynamic asymmetry faults being studied in this research. Section III introduces the Continuous Wavelet Transform and provides background

978-1-7281-1981-6/19/$31.00 ©2019 IEEE

Authorized licensed use limited to: Florida Atlantic University. Downloaded on July 27,2020 at 18:30:18 UTC from IEEE Xplore. Restrictions apply.

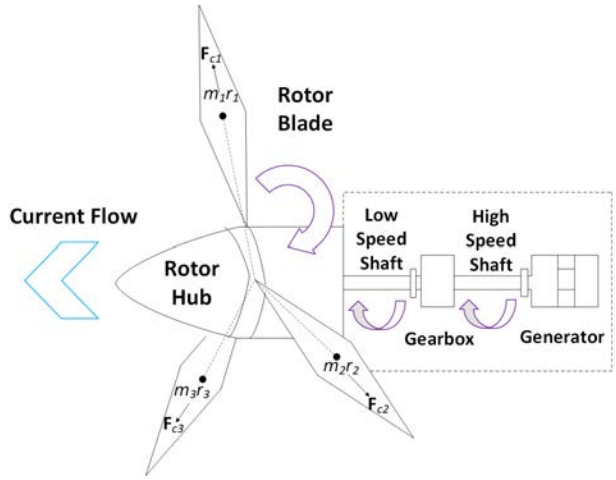

Fig. 1. Simplified model of a 3-bladed MHK turbine. Fault energy experienced by the rotor blades is transferred to the rotor shaft.

information on Morlet Wavelets. Section IV summarizes experiments performed in this research and quantifies their results. Lastly, concluding remarks and suggestions for future research is presented in section V.

II. MHK Turbine Modeling and Simulation

A. Simulation Platform Overview

The simulation platform used in this research integrates NREL's Fatigue, Aerodynamics, Structures, and Turbulence (FAST) simulation suite inside of MATLAB & Simulink [10]–[12]. This platform is configured to numerically simulate the dynamics of a 20 kW, 3-bladed, horizontal axis MHK turbine, and induce upon it realistically modeled marine hydrodynamic operating conditions.

This platform is configured to model full field turbulent marine current conditions using NRELs TurbSim stochastic inflow turbulence tool [13]. The input files are generated using the TIDAL-spectral model, along with a mean current speed of 1.90 m/s, and a turbulence intensity of 5% to simulate ocean currents. The TIDAL-spectral model is based upon measurements taken from a tidally mixed channel near Marrowstone Island in Puget Sound, Washington [14].

B. Blade Imbalance-induced Hydrodynamic Asymmetry Faults

As with conventional wind turbines, rotor blade imbalance faults will likely be some of the most prevalent types of faults impacting MHK turbines. Such imbalances can arise from either a defect that occurred during the manufacturing and construction phases of the turbine, or develop during normal operation due to the accumulation of wear and tear.

In cases where the pitch angle of one blade is deviated to the extent that its angle of attack causes it to have differing hydrodynamic behaviors from the other two blades may cause hydrodynamic asymmetry faults to arise. As the turbine's rotor begins to rotate under this unbalanced condition, an unbalanced hydrodynamic moment is induced upon the rotor shaft. For homogeneous current inflow conditions, the introduction of this moment does not directly impact the production of

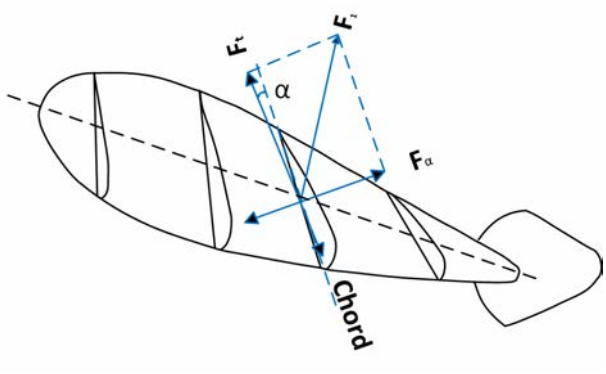

Fig. 2. Simple representation of a healthy rotor blade. The pitch angle of the blade and its angle of attack, α, are intact and in proper working order.

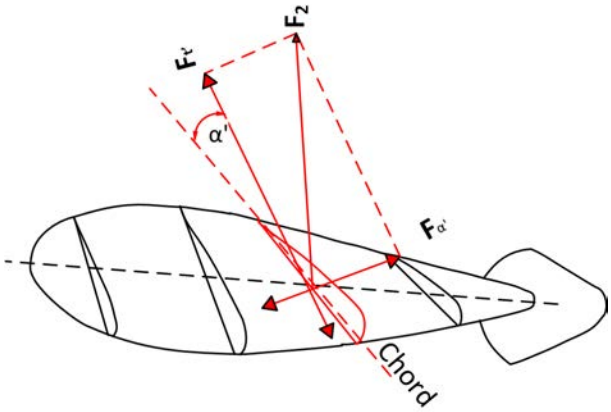

Fig. 3. Simple representation of a faulty propeller blade. The pitch angle of the blade is deviated, and thus the angle of attack, α', is also deviated. This deviation of α imparts unbalanced moments of inertia and torques onto the turbine's rotor shaft.

power, since the net hydrodynamic torque remains constant. However, the vertical current shear that naturally occurs in rivers, tidal flows, and ocean currents will interact with this asymmetry creating rotor torque fluctuation that are introduced into the system at the 1P frequency.

Depicted in Fig. 2 is a simplified representation of a healthy rotor blade, in which the angle of attack is labeled as α. In healthy conditions, axial hydrodynamic forces, $\mathbf{F}_a$, are induced upon the rotor blade, and tangent forces, $\mathbf{F}_t$, induced torque upon the rotor shaft. During rotation, if the pitch angle (and thus the angle of attack) of one of the blades is out of alignment with that of the other two blades, unbalanced hydrodynamic forces $\mathbf{F}_{a'}$, and $\mathbf{F}_{t'}$, will be invoked upon the misaligned blade, as shown in Fig. 3. These newly created hydrodynamic forces impart unaccounted for torques and moments of inertia onto the misaligned blade. The introduction of the kinetic energy that is coupled within these unaccounted for moments and torques are what produce the dynamic loads and vibrations that are transferred onto the rotor shaft [15]. This transfer of energy onto the rotor shaft is also visible within the frequency spectra of the generator's output power at the 1P shaft rotating frequency.

Authorized licensed use limited to: Florida Atlantic University. Downloaded on July 27,2020 at 18:30:18 UTC from IEEE Xplore. Restrictions apply.

III. Wavelet Transform Theoretical Background

The wavelet transform can be interpreted as the convolution between a signal, $x(t)$, and a wavelet basis function, $\Psi(t)$. The signal $x(t)$ can be any measurement from the turbine, however for the purposes of this research, $x(t)$ represents the generator power signal, which in itself, is an easily collectible non-intrusive signal. $\Psi(t)$, also known as the mother wavelet, is the function for which dilated and translated versions of itself are derived and used inside of the wavelet transform [16]. Wavelets are small, localized wave-like functions of oscillatory nature, that have finite energy, zero mean, and who posses Fourier Transforms that vanish for negative frequencies [7], [16].

In general, there is a wide variety of mother wavelet basis functions that can be used for the analysis of data. The optimal choice is largely dependent upon both the nature of the signal being analyzed and the characteristics of the phenomena being researched. The Morlet wavelet was selected as the mother wavelet of choice for this research. More insights upon why this wavelet was chosen will be expanded upon in part B of this section.

A. Continuous Time Wavelet Transform

There are two hyper-parameters that can be manipulated to make $\Psi(t)$ more robust for signal analysis. $\Psi(t)$ can be stretched or squeezed (dilated), or it can be shifted along the time axis (translated). Dilations of $\Psi(t)$ are controlled by the dilation parameter, **a**, while translations are controlled by the translation parameter **b**.

For a shifted and dilated version of $\Psi(t)$, the form:

$$\Psi(t) = \Psi\left(\frac{t-b}{a}\right) \tag{1}$$

may be used. The wavelet transform of a continuous signal, $x(t)$, that utilizes a range of **a**'s and **b**'s can be defined as:

$$\mathbf{T}(a,b) = w(a)\int_{-\infty}^{\infty} x(t)\Psi^*\left(\frac{t-b}{a}\right)dt \tag{2}$$

where the products of the signal being analyzed and the shifted and dilated wavelet functions are called the wavelet coefficients, $\mathbf{T}(a,b)$. The wavelet coefficients can be thought of as measures of cross-correlation between the signal, $x(t)$, and a set of wavelets of various dilations [16]. In (2), $w(a)$ is a weighting function that is customarily set equal to $1/\sqrt{a}$, to ensure that wavelets of the same scale all posses an equal amount of energy. Lastly, the * symbol is used to indicate that the complex conjugate of the wavelet basis function is utilized within the wavelet transform.

From here, it is advantageous to show how the convolution theorem can be use to express the wavelet transform as the result of the inner product between the Fourier Transforms of the signal, $\hat{x}(f)$, and that of the wavelet, $\hat{\Psi}_{a,b}(f)$:

$$\mathbf{T}(a,b) = \int_{-\infty}^{\infty} \hat{x}(f)\,\hat{\Psi}^*_{a,b}(f)\,df \tag{3}$$

For a dilated and translated version of the wavelet, the Fourier Transforms yields:

$$\hat{\Psi}_{a,b}(f) = \int_{-\infty}^{\infty} \frac{1}{\sqrt{a}}\Psi\left(\frac{t-b}{a}\right)e^{-i(2\pi f)t}dt \tag{4}$$

After implementing the substitution $t'= (t-b)/a$, such that $dt = adt'$, the Fourier Transform of $\hat{\Psi}_{a,b}(f)$ becomes:

$$\hat{\Psi}_{a,b}(f) = \frac{1}{\sqrt{a}}\int_{-\infty}^{\infty} \Psi(t')e^{-i(2\pi f)(at'+b)}adt' \tag{5}$$

Further simplification of $\hat{\Psi}_{a,b}(f)$ via the factorization of the constant exponential term out of the integral and the re-substitution of t' back to t yields:

$$\hat{\Psi}_{a,b}(f) = \sqrt{a}e^{-i(2\pi f)(b)}\int_{-\infty}^{\infty} \Psi(t)e^{-i(2\pi f)t}dt \tag{6}$$

Thus it can be seen that the integral expression in (6) is equation (4) re-scaled at frequency af, and thus, (5) can be rewritten as:

$$\hat{\Psi}_{a,b}(f) = \sqrt{a}\,\hat{\Psi}(af)e^{-i(2\pi f)b} \tag{7}$$

With the Fourier Transform of the translated and dilated version of the wavelet having now been defined, the complex conjugate form can be written as:

$$\hat{\Psi}^*_{a,b}(f) = \sqrt{a}\,\hat{\Psi}^*(af)e^{-i(2\pi f)b} \tag{8}$$

In conclusion, Equation (4) can now be expressed as:

$$\mathbf{T}(a,b) = \sqrt{a}\int_{-\infty}^{\infty} \hat{x}(f)\,\hat{\Psi}^*(af)e^{-i(2\pi f)b}df \tag{9}$$

with the deviations of Equations (1-10) coming courtesy of [16].

The wavelet coefficient values, $\mathbf{T}(a,b)$, are usually mapped onto a 2-dimensional plane in which the axes are measures of the various translations and scales of the mother wavelet basis function. When the shape of the wavelet at a specific translation and scale has a high correlation with the shape of the signal that it is analyzing, a greater wavelet coefficient value is produced. Similarly, when the shape of the wavelet of a specific translation and scale has a lower correlation with the shape of the analyzed signal, a smaller wavelet coefficient value is produced.

Traditionally, this mapping can be executed in a smooth and continuous fashion (i.e. CWT), and allows for a more succinct visualization of the correlation between the wavelet and the signal under analyzation [16].

B. Complex Morlet Wavelet

A core tenet of the inner product theory is the idea that any signal can be expressed as a linear combination of a set of basis functions. This principle provides an extremely vital benefit for RMFD and diagnosis when using wavelets as opposed to sinusoids as basis functions [8]. Since the performance of RMFD lies within the ability to match the shape of the wavelet basis function to the shape characteristics of a particular fault features contained within a signal, choosing an optimal

Authorized licensed use limited to: Florida Atlantic University. Downloaded on July 27,2020 at 18:30:18 UTC from IEEE Xplore. Restrictions apply.

mother wavelet function is imperative for accurate condition monitoring and fault detection.

For the purposes of this research a Morlet wavelet is selected as the mother wavelet basis function. The reason for this selection is due to the unique way in which Morlet wavelets are able to localize the frequency information of $x(t)$ in time. The increased control and precision that the shape of their windowing kernel allows for in the frequency domain makes them logical choices for analyzing frequency band specific activity [17].

A complex Morlet wavelet can be constructed by tapering a sine wave with a Gaussian window function. This can be achieved by multiplying the Gaussian function with the sine wave as shown:

$$w = e^{2i\pi ft} e^{\left(\frac{-t^2}{2(\sigma)^2}\right)} \tag{10}$$

where i is the imaginary operator, f is the peak frequency in Hertz of the sine wave, and t is the time in seconds. When selecting t, the inclusion of a phase shift can be bypassed by selecting a time range that centers t at zero, such that: $-t \leq 0 \leq t$ [9].

Multiple sine waves of differing frequencies are used to construct the Morlet Wavelets that are used to analyze $x(t)$. This is synonymous to Fourier Transform analysis, in which multiple sine waves are also used to preform frequency domain analyses on $x(t)$. However, unlike the sine waves of the Fourier Transform, time-frequency decomposition via wavelet convolution allows for the specification of the frequencies used to construct the Morlet wavelets to be chosen manually, as opposed to being dictated by the number of time series data points contained within $x(t)$ [17]. For this research, the 1P shaft rotating frequency is of interest, and therefore a frequency range ranging from 0.1Hz to 2Hz is selected for analysis.

The parameter that controls the width of the Gaussian window in (10) is σ, which is calculated as:

$$\sigma = \frac{n}{2\pi f} \tag{11}$$

where n dictates the trade off between frequency and time precision. This is an extremely non-trivial parameter that controls the Heisenberg uncertainty principle for time-frequency analysis, in that it is not possible to concurrently achieve both optimal time and frequency precision [17]. The selection of n heavily influences the quality of results that are achievable from the data.

Larger values of n provides a better frequency precision at the expense of decreased temporal precision, while the opposite is true for smaller values of n. Thus, smaller values of n are better for transient activity analysis, while larger values of n are better for longer excitation activity [17]. Since this research is concerned with analyzing frequency excitations around the 1P shaft rotational frequency, larger values of n were of interest. Through trial and error, a range between 5 to 15 was selected for n, with 500 increments between the min and max values of n.

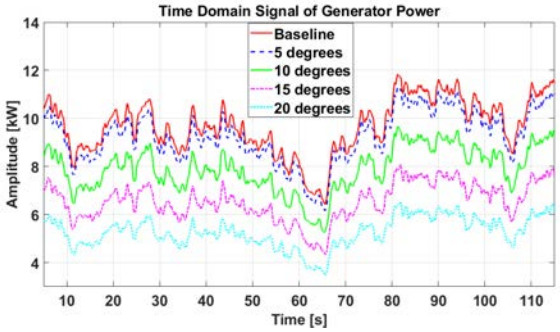

Fig. 4. Time domain representation of generator output power for all pitch deviation fault scenarios. An initial two minute simulation was run, in which only the time period interval from 5-115 seconds was used.

IV. Experimental Design and Results

In total, 5 different current spectral seeds are tested, for which a tidal intensity value of 5% is used in each seed. It should be noted that a time window long enough to capture a suitable amount of data will be necessary to determine the average rotating frequency of the rotor shaft. For the purposes of this research 2 minute time histories are utilized. Since FAST makes it possible to determine the instantaneous frequency of the rotor, this stipulation is less of a concern. However, outside of a laboratory environment, this stipulation will need to be met in order to reproduce the methods presented in these experiments.

Fig. 4 presents the time domain representation of the generator output power for a typical current spectral seed. A baseline case is initially simulated, in which no pitch angle deviation faults are induced upon the rotor blades. Similar simulations are then run and plotted for pitch angel deviations of 5, 10, 15, and 20 degrees. For the baseline case, the MHK turbine has a rotational speed of 60 RPMs (1 Hz).

A. Spectrum Analysis

The top portion of Fig. 5 is a spectrogram representation of the electrical power output of the turbine's generator, corresponding to the 20 degree pitch fault case. The spectral image was generated using a CWT with a Morlet basis function. The instantaneous frequency of the rotor is overlaid on top of the spectral image (represented by the solid white line). Since the original generator power output was sampled according to a normal distribution, 99.7% of all frequency band specific activity corresponding to the 1P frequency region of interest is bound within a range of +/- 3 standard deviations (3-STD) of the instantaneous rotating frequency of the rotor shaft (highlighted by the two dotted white lines).

The plot underneath the spectrogram is an attempt to use the PSD to quantify the frequency band activity between the +/- 3-STD range. The PSD graph sums up the normalized wavelet coefficient energy for specific frequency scales of the wavelets. This measure can be thought of as the amount of relative signal energy per specific translation point and frequency scale of the wavelet. The solid line represents the average rotating frequency of the rotor shaft, and the dotted lines on either side

Authorized licensed use limited to: Florida Atlantic University. Downloaded on July 27,2020 at 18:30:18 UTC from IEEE Xplore. Restrictions apply.

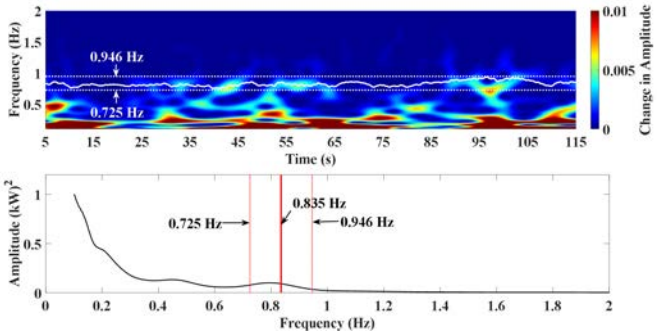

Fig. 5. Top: Spectrogram representation of the generator output power for the 20 degree pitch fault scenario. The instantaneous 1P frequency (solid white line) is range bounded by +/- 3-STD of the instantaneous frequency (dotted white lines). Bottom: PSD of the generator output power. The average rotating frequency of the rotor shaft (solid line) is range bounded by +/- 3-STD of the instantaneous rotor frequency (dotted red lines).

TABLE I
FREQUENCY BOUNDS FOR SHAFT 1P ROTATING FREQUENCY AND MEAN FAULT ENERGY

Pitch Angle	Avg Freq.±3-STD	**Mean Energy**	Mean Energy STD
Baseline	1.012±0.134	**1.701**	0.627
5 Degrees	0.997±0.132	**1.772**	0.698
10 Degrees	0.946±0.127	**2.815**	1.105
15 Degrees	0.888±0.119	**3.568**	1.340
20 Degrees	0.835±0.110	**5.305**	2.125

of the average frequency line correspond to the boundaries of the +/- 3-STD frequency range. From the figure, a distinct amount of energy is observed in the range.

B. Quantification of Results

As shown within both the spectral image and PSD plot, frequency excitations within the +/- 3-STD range do start to become more prevalent as the pitch angle deviations increase. This can be verified by noticing the frequency excitation blips shown within this range on the spectrogram plot, and by Table I, which sums up the wavelet coefficient energy within the +/- 3-STD range of the 1P frequency of the rotor shaft for all pitch angle imbalance fault scenarios. As portrayed in Table I, a steady increase in the wavelet coefficient fault energy can be observed within this frequency range of interest. These quantified fault features can further be used for MHK hydrodynamic asymmetry faults detection.

V. CONCLUSIONS AND FUTURE WORK

In this research, the dynamics of hydrodynamic asymmetry faults induced upon the rotor blades of a MHK turbine were studied for the purpose of evaluating non-intrusive fault analysis methods. A continuous wavelet transform (CWT) with a complex Morlet wavelet basis function was used to experimentally verify that frequency excitations within the +/- 3-STD region of the rotor shaft's 1P frequency could indeed be visualized and quantitatively analyzed in the frequency spectrum of the generator's electrical power signal.

Moving forward, future works should focus on ways to adaptively optimize the Morlet Wavelet to better match generator power signals. Additionally, fault detection system will be developed based on machine learning techniques (e.g, deep learning) using the quantified fault signatures from this paper.

ACKNOWLEDGMENT

This work was supported by the Walter & Lalita Janke Foundation and the National Science Foundation under grant ECCS-1809164. We would also like to thank Drs. Hassan Mahfuz and Takuya Suzuki for providing their FAST models, Broc Dunlap and David Wilson for preparing the TurbSim and simulation data, and Mike X Cohen for his aid with utilizing complex Morlet Wavelets within MATLAB.

REFERENCES

[1] "Renewable Electricity Futures Study," https://www.nrel.gov/analysis/re-futures.html, accessed: 2018-10-30.

[2] T. Mai, R. Wiser, D. Sandor, G. Brinkman, G. Heath, P. Denholm, D. Hostick, N. Darghouth, A. Schlosser, and K. Strzepek, "Renewable electricity futures study. volume 1: Exploration of high-penetration renewable electricity futures," Department of Energy, Tech. Rep., June 2012.

[3] K. Haas, "Assessment of energy production potential from ocean currents along the united states coastline," Georgia Tech Research Corporation, Tech. Rep., 2013.

[4] X. Gong and W. Qiao, "Imbalance fault detection of direct-drive wind turbines using generator current signals," *IEEE Transactions on energy conversion*, vol. 27, no. 2, pp. 468–476, 2012.

[5] ——, "Current-based mechanical fault detection for direct-drive wind turbines via synchronous sampling and impulse detection," *IEEE Transactions on Industrial Electronics*, vol. 62, no. 3, pp. 1693–1702, 2015.

[6] M. Riera-Guasp, J. Pons-Llinares, V. Climente-Alarcon, F. Vedreño-Santos, M. Pineda-Sánchez, J. Antonino-Daviu, R. Puche-Panadero, J. Perez-Cruz, and J. Roger-Folch, "Diagnosis of induction machines under non-stationary conditions: Concepts and tools," in *Electrical Machines Design Control and Diagnosis (WEMDCD), 2013 IEEE Workshop on*. IEEE, 2013, pp. 220–231.

[7] R. Yan, R. X. Gao, and X. Chen, "Wavelets for fault diagnosis of rotary machines: A review with applications," *Signal Processing*, vol. 96, pp. 1–15, 2014.

[8] J. Chen, Z. Li, J. Pan, G. Chen, Y. Zi, J. Yuan, B. Chen, and Z. He, "Wavelet transform based on inner product in fault diagnosis of rotating machinery: A review," *Mechanical systems and signal processing*, vol. 70, pp. 1–35, 2016.

[9] M. X. Cohen, "A better way to define and describe morlet wavelets for time-frequency analysis," *bioRxiv*, 2018. [Online]. Available: https://www.biorxiv.org/content/early/2018/08/21/397182

[10] J. M. Jonkman, M. L. Buhl Jr *et al.*, "Fast users guide," National Renewable Energy Laboratory, Tech. Rep., 2005.

[11] Y. Tang, J. VanZwieten, B. Dunlap, D. Wilson, C. Sultan, and N. Xiros, "In-stream hydrokinetic turbine fault detection and fault tolerant control - a benchmark model," in *American Control Conference (ACC), 2019*. IEEE, 2019 (Submitted).

[12] D. Wilson, P. Passmore, Y. Tang, and J. VanZwieten, "Bidirectional long short-term memory networks for rapid fault detection in marine hydrokinetic turbines," in *17th IEEE International Conference On Machine Learning And Applications (ICMLA), 2018*. IEEE, 2018 (Accepted).

[13] "Marine hydrokinetics - nwtc information portal," https://nwtc.nrel.gov/technology-type/marine-hydrokinetics.

[14] J. Thomson, B. Polagye, V. Durgesh, and M. C. Richmond, "Measurements of turbulence at two tidal energy sites in puget sound, wa," *IEEE Journal of Oceanic Engineering*, vol. 37, no. 3, pp. 363–374, 2012.

[15] D. Jiang, Q. Huang, and L. Hong, "Theoretical and experimental study on wind wheel unbalance for a wind turbine," in *2009 World Non-Grid-Connected Wind Power and Energy Conference*, Sept 2009.

[16] P. S. Addison, *The illustrated wavelet transform handbook: introductory theory and applications in science, engineering, medicine and finance*. CRC press, 2017.

[17] M. X. Cohen, *Analyzing neural time series data: theory and practice*. MIT press, 2014.

Authorized licensed use limited to: Florida Atlantic University. Downloaded on July 27,2020 at 18:30:18 UTC from IEEE Xplore. Restrictions apply.